Assessment of chemo-mechanical degradation of concrete sewer pipes through an integrated experimental approach

Document license:
CC BY

DOI:
10.1016/j.engstruct.2023.116590

Document status and date:
Published: 15/10/2023

Document Version:
Publisher's PDF, also known as Version of Record (includes final page, issue and volume numbers)

Please check the document version of this publication:

• A submitted manuscript is the version of the article upon submission and before peer-review. There can be important differences between the submitted version and the official published version of record. People interested in the research are advised to contact the author for the final version of the publication, or visit the DOI to the publisher's website.
• The final author version and the galley proof are versions of the publication after peer review.
• The final published version features the final layout of the paper including the volume, issue and page numbers.

Link to publication

Download date: 04. Oct. 2023

Assessment of chemo-mechanical degradation of concrete sewer pipes through an integrated experimental approach

R.A. Luimes [a], I.C. Scheperboer [a], A.S.J. Suiker [a],[*], E. Bosco [a], F.H.L.R. Clemens [b,c]

[a] *Department of the Built Environment, Eindhoven University of Technology, P.O. Box 513, 5600 MB Eindhoven, The Netherlands*
[b] *Department of Hydraulic Engineering, Deltares, P.O. Box 177, 2600 MH Delft, The Netherlands*
[c] *Department of Civil and Environmental Engineering, Norwegian University of Science and Technology, P.O. Box 8900, NO-7491, Trondheim, Norway*

ARTICLE INFO

ABSTRACT

The chemo-mechanical degradation of unreinforced concrete sewer pipes applied in domestic service locations is assessed through a systematic, integrated experimental approach, considering 18 new and 35 used sewer pipes. The characteristics and environmental conditions of the sewer pipes are reported, and data obtained from surface condition classification, residual alkalinity tests and XRD analyses are combined to identify the type and degree of chemical attack of the used sewer pipes. Concrete material properties are determined by material tests on sewer pipe samples, providing quantitative insight into the age dependency of the Young's modulus, compressive strength, tensile strength and mode I toughness. All relatively old pipes (installed in the 1920s and 1950s) show substantial chemical attack by biogenic sulphide corrosion (at the inner side of the pipe) and carbonation (at the outer side of the pipe). The time development of the corresponding corrosion depths on average follows a linear trend, whereby the corrosion rate for biogenic sulphide corrosion is about a factor of 1.3 larger than for carbonation. Due to these chemical processes, the mechanical properties of concrete may significantly depend on the age of the sewer pipe. In particular, the average compressive strength and average tensile strength decrease approximately linearly with the age of the pipe, in correspondence with relative reductions of, respectively, a factor of 1.7 and 1.5 over a period of almost 100 years. The values and time-dependent trends found for the concrete properties and corrosion depths of sewer pipes can serve as input for practical analyses and advanced numerical simulations on their bearing capacity and time-dependent degradation. The experimental results also emphasize the importance of regularly assessing the amount of chemical degradation of (especially older) *in-situ* sewer pipes, by determining the (decrease in) effective wall thickness via core sampling and laser profiling.

1. Introduction

The degradation of the sewerage infrastructure has a major impact on the society and environment, and leads to high financial costs. The replacement value of the sewer network in The Netherlands has been estimated to be approximately €58 billion, which has to be covered by household and company taxes [1,2]. In order to make an appropriate choice between avoiding the risk of catastrophic sewer collapse and premature, capital-intensive replacement of the sewer network, adequate sewer asset management is essential, requiring an accurate assessment of the structural condition of *in-situ* sewer pipes [2]. At present, the most common approach for assessing the structural condition of sewer systems is by visual inspection of the accessible inside of pipes via closed-circuit television (CCTV), followed by manually classifying the condition using dedicated standards [3–5]. However, the accuracy and reliability of the results obtained from this method often

turn out to be questionable, as approximately 25% of the damage may remain undetected [3] and no evident correlation exists between the visual inspection data and the actual material properties of the sewer pipes [2,6]. In addition, the influence by biochemical processes on the structural integrity of sewer pipes is left out of consideration [4,7].

In the literature, several biochemical processes have been identified that are responsible for the degradation of concrete sewer systems. The most relevant degradation process is *biogenic sulphide corrosion* [8–14]. In this process, the aerobic bacteria present in the thin water film at the inner pipe surface convert the dissolved ionic species of the hydrogen sulphide gas released by the wastewater into sulphuric acid, which reacts with the calcium hydroxide and, subsequently, with the calcium silicate hydrate that are dissolved in the pore structure of the concrete, eventually resulting in the formation of gypsum [15,16]. Gypsum, in

principle, may be further converted into ettringite, but ettringites are chemically unstable in acidic environments and dissolve relatively fast, so that they are less frequently observed under *in-situ* conditions typical of sewer pipe systems [17,18]. Biogenic sulphide corrosion affects the mechanical integrity of sewer pipes, as it leads to an increase of the concrete porosity [18–21] and, accordingly, to a decrease in strength and stiffness properties [12,17,22–24]. The degradation rate hereby depends on factors such as the hydrogen sulphide gas concentration, the availability of nutrients for the aerobic bacteria, and the relative humidity and gas temperature of the sewer pipes' atmosphere [13,14]. At the outer pipe surface, degradation is typically caused by corrosion under sulphate attack, acid attack (e.g., humic acid or carbonic acid), microbial action or carbonation [22,25]. Specific environmental conditions, such as the presence of soil pollutants, anaerobic conditions and low temperatures, may accelerate these chemical processes [22]. *Carbonation* hereby occurs most frequently, and originates from the diffusion of carbon dioxide (naturally present in soil) towards the outer surface of concrete sewer pipes, at which it can react with hydrated cement in the presence of moisture. This process may lead to changes in the strength, porosity and pore size distribution of the cement paste [22,25]. In addition to chemical processes, degradation of sewer pipes may also be caused by backfilling procedures [26–28], installation practices [8,29,30], the presence of erosion voids [31–35], and (heavy) traffic loading [30,36]. These factors can unfavourably affect the soil–pipe interaction, potentially leading to damage and catastrophic failure of the sewer system [37].

In order to support the development of a more solid basis for the assessment and prediction of the structural condition of concrete sewer systems, in the present paper the chemo-mechanical degradation of unreinforced concrete sewer pipes applied in domestic service locations is systematically assessed through an integrated experimental approach, considering 18 new and 35 used sewer pipes. The characteristics and *in-situ* conditions of the sewer pipes are documented, and a classification system is developed for the inner and outer surface conditions of the sewer pipes. Further, an accurate quantification of the residual alkalinity of the sewer pipe cross-section is performed, and the past occurrence of chemical attack is revealed by means of X-ray diffraction (XRD) analyses. The results from these analyses allow for identifying the type and amount of chemical corrosion. The time-dependency of the amount of chemical corrosion is determined by establishing a trend between the age of the pipe and the corrosion depth across the pipe wall. In addition, dedicated material experiments are performed on concrete samples taken from the sewer pipes for determining the Young's modulus, compressive strength, tensile strength and mode I toughness. From these results, trend lines are constructed that illustrate how these mechanical properties vary with the age of the sewer pipe. The values and time-dependent trends found for the concrete properties and corrosion depths of sewer pipes may serve as input for practical analyses and advanced numerical simulations on their bearing capacity and time-dependent degradation, see for example, [37,38].

The paper is organized as follows. Section 2 presents an overview of the experimental program by describing the investigated concrete sewer pipes and the methodologies proposed for the assessment of the type and degree of chemical attack and material properties of the sewer pipes. The experimental results are presented and combined in Section 3, whereby the extent of deterioration of the sewer pipes is correlated to the material properties and their age. The main conclusions and practical recommendations following from the experimental research are summarized in Section 4.

2. Experimental program

In the experimental program, 18 new sewer pipes and 35 used sewer pipes applied in domestic service locations are examined. All sewer pipes are dry-cast and unreinforced. In Section 2.1 an overview of the age and geometrical and material characteristics of the sewer pipes is provided, as well as a specification of the traffic loading and the *in-situ* soil conditions the used pipes were exposed to during their service life. Sections 2.2 and 2.3 respectively treat the methodologies to assess the extent of deterioration and the mechanical material properties of the sewer pipes.

2.1. Concrete sewer pipes

2.1.1. Sewer pipe characteristics

Table 1 presents a summary of the characteristics of the 18 new and 35 used unreinforced, dry-cast concrete sewer pipes considered in the experimental program. The sewer pipes are labelled with an identity code (IC) presented in the first column of the table, which refers to their geometry, dimensions, year of installation and domestic service location. Depending on the availability, the total number of pipe specimens varies between 2 and 6. Round and egg-shaped geometries were selected, for which the width ranges between 300–800 mm and the height between 400–1200 mm, respectively, see also the examples depicted in Fig. 1. The final number in the IC used in the caption of Fig. 1 refers to a specific sewer pipe specimen, which may vary between 1 and the total number of tested pipe specimens, as listed in the 6th column of Table 1. The new sewer pipes were manufactured by the production companies Kijlstra and De Hamer, located in The Netherlands, and serve as the *reference case* of "pipes without damage". The new round and egg-shaped pipes were designed according to pipe strength classes 135 and 250, respectively, whereby the concrete composition complies with environmental class XA3 according to NEN-EN 206 [39]. This concrete composition is characterized by a maximum water-cement ratio of 0.45, a minimum amount of cement of 340 kg/m^3, and a minimum strength class of C35/45. The used sewer pipes, with an age up to 95 years, had been in service as a combined domestic sewer system (i.e., the pipes installed in the 1920s and 1950s) or as an improved, separated domestic sewer system (i.e., the pipes installed in the 1990s) up to July/August 2019 (pipes from Arnhem) and January 2020 (pipes from The Hague). Although detailed information on the composition and time-dependent variations of the wastewater is not available for the tested sewer pipes, considering their domestic service locations it may be expected that the sewer systems have not been (significantly) exposed to industrial, corrosive chemicals (which may enlarge the rate of degradation). Further, the sewer systems have not been subjected to rehabilitation or protection treatments.

Traditionally, dry-cast concrete sewer pipes are composed of a mixture of Portland cement, fine sand aggregates, course gravel aggregates and water, with a maximum water-cement ratio of 0.40, whereby the concrete is carefully compacted to fulfil strict requirements regarding water tightness and chemical resistance [12,23,40–42]. Only in cases where a high risk of sulphate attack is expected, a more sulphate resistant cement type is advised to be used [42]. Such circumstances are occasionally observed at connections between pressurized sewers and gravity sewers, in turbulent sewer atmospheres, or in sewer systems applied in industrial areas [9,42,43], and thus do not apply to the domestic sewer pipes studied in this paper.

2.1.2. Traffic loading and in-situ soil conditions

During service, the concrete sewer pipes were exposed to the traffic loading and *in-situ* soil conditions specified in Table 2; this information has been obtained from the municipalities of Arnhem and The Hague, and from publicly available inspection reports. The sewer pipes were located in domestic areas characterized by mild car traffic with a maximum speed of 30 or 50 km/h, with the occasional passage of larger vehicles (trucks, buses) at some of the locations. At the service locations in Arnhem, the sewer pipes were embedded within a sand layer, or a combination of clay and sand layers. At the service locations in The Hague, the sewer pipes were embedded in a sand or a peat layer. In two cases the pipes were installed above the ground water level, and in seven cases below the ground water level. Further, mild concentrations

Table 1

Specifications of the sewer pipe types considered in the experimental program. The first column indicates the identity code (IC), which is used to refer to a specific sewer pipe type. The labelling system corresponds to the data presented in the second to fifth column of the table, which consists of (i) a letter "R" or "E" referring to a round or egg-shaped geometry, respectively, (ii) the global dimensions of the sewer pipe as denoted by the inner width and height (in mm × mm), (iii) the year of installation, and (iv) the first letter(s) of the name of the municipality where the sewer pipe had been in service, using "A" for Arnhem and "TH" for The Hague, or the indication that the pipe is "new". The last two columns list the number of tested pipe specimens and the average wall thickness (in mm), respectively. For the egg-shaped pipes, the average wall thickness refers to the upper half of the pipe cross-section.

IC	Geometry	Dimensions (mm × mm)	Year of installation	Service location	Number of pipes	Wall thickness (mm)
R400-2015-new	Round	400 × 400	–	–	6	63
R400-1924-A	Round	400 × 400	1924	Arnhem	4	54
R500-2015-new	Round	500 × 500	–	–	6	71
R500-1997-A	Round	500 × 500	1997	Arnhem	2	68
R700-1996-A	Round	700 × 700	1996	Arnhem	4	96
E300/450-1951-TH	Egg-shaped	300 × 450	1951	The Hague	6	52
E300/450-1926-TH	Egg-shaped	300 × 450	1926	The Hague	5	57
E400/600-2015-new	Egg-shaped	400 × 600	–	–	6	68
E400/600-1951-TH	Egg-shaped	400 × 600	1951	The Hague	2	72
E400/600-1924-TH	Egg-shaped	400 × 600	1924	The Hague	5	72
E400/600-1924-A	Egg-shaped	400 × 600	1924	Arnhem	4	58
E800/1200–1954-A	Egg-shaped	800 × 1200	1954	Arnhem	3	136

(a) R400-1924-A-2   (b) R500-1997-A-2

(c) E300/450-1926-TH-3   (d) E400/600-1924-A-3   (e) E800/1200-1954-A-3

Fig. 1. A selection of unreinforced, used concrete sewer pipe specimens considered in the experimental program. Different surface conditions can be identified at the inner surface of the sewer pipes.

of soil pollutants were occasionally present, such as mercury, lead, mineral oil, molybdenum, barium and benzene, which are believed to not have had a serious effect on the pipe condition. Finally, it is noted that the available information on the local soil profiles was insufficient to assess the effect of differential settlements on the integrity of a pipe; therefore, this effect has not been considered in this study.

2.2. Assessment of deterioration

The degree of deterioration of the 35 used sewer pipes has been classified in terms of the surface conditions, in accordance with the classification system described in Section 2.2.1. The chemical attack of the pipes was analysed by the residual alkalinity tests and XRD analyses described in Sections 2.2.2 and 2.2.3, respectively.

2.2.1. Classification of pipe surface conditions

The used sewer pipe specimens were subjected to a visual inspection procedure, whereby the degree of deterioration was determined in accordance with a classification system based on specific surface conditions. Accordingly, 6 different surface condition classes were identified, which are denoted using common terminology adopted in the sewer asset management community [44], see Table 3. For the inner pipe surface, the 4 relevant surface condition classes are: *Smooth*, *Exposed granulates*, *Porous mortar between granulates* and *Deposits - Dark coloured bands*. For the outer pipe surface, the 4 relevant classes are: *Smooth*, *Rough*, *Exposed granulates* and *Excavation damage*. Here, the class *Smooth* corresponds to an (almost) intact surface that is similar to the surface of a new sewer pipe. The surface class *Exposed granulates* refers to a surface that has been exposed to chemical attack, whereby the outer mortar layer has spalled off and the larger granulates have become
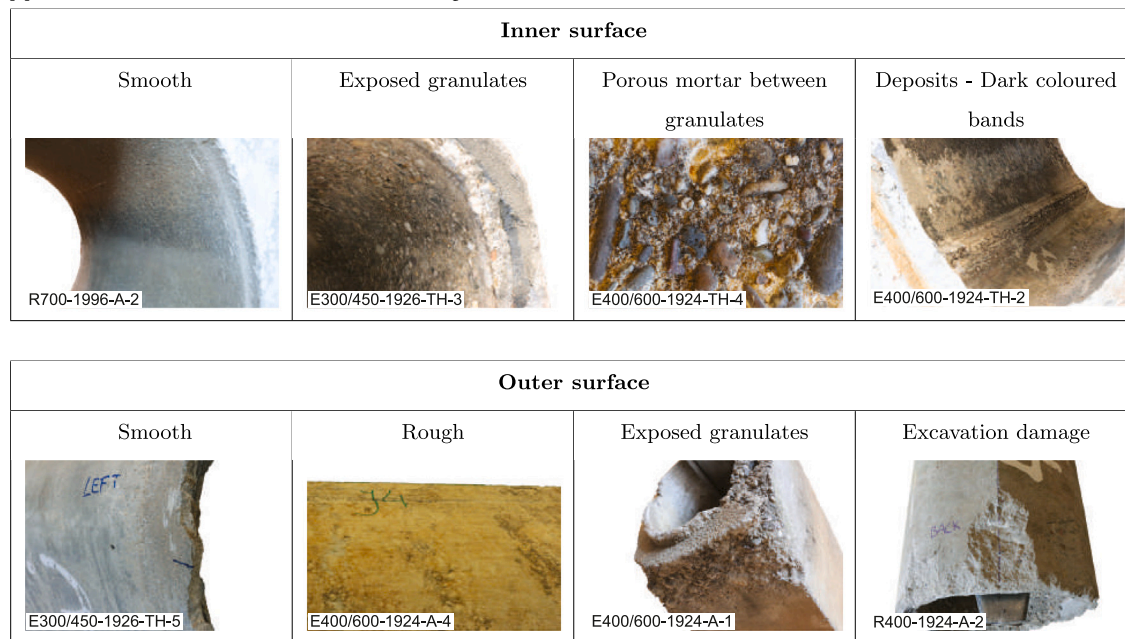
Table 2

Specifications of traffic loading and *in-situ* soil conditions experienced by the used sewer pipes during their service life in a domestic service location. The soil pollutants mercury (ME), lead (L), mineral oil (MOil), molybdenum (MO), barium (BA) and benzene (BE), were occasionally present in mild concentrations.

IC	Traffic			Soil		
	Domestic area	Max speed (km/h)	Passage large vehicles	Soil embedment	Ground water level	Soil pollutants
R400-1924-A	Yes - main road	50	Trucks + buses	Sand	Below pipe	ME
R500-1997-A	Yes	30	–	Clay/sand	Above pipe	–
R700-1996-A	Yes	30	–	Clay/sand	Above pipe	–
E300/450-1951-TH	Yes	30	–	Peat	Above pipe	ME-L-MOil-MO
E300/450-1926-TH	Yes	30	–	Sand	Above pipe	–
E400/600-1951-TH	Yes	30	–	Peat	Above pipe	ME-L-MOil-MO
E400/600-1924-TH	Yes	30	–	Sand	Above pipe	–
E400/600-1924-A	Yes - main road	50	Trucks + buses	Sand	Below pipe	ME-L
E800/1200–1954-A	Yes - city centre	50	Trucks	Sand	Above pipe	MO-BA-BE

Table 3

Representations of the 6 surface condition classes: (1) Smooth, (2) Exposed granulates, (3) Porous mortar between granulates, (4) Deposits - Dark coloured bands, (5) Rough, and (6) Excavation damage, as observed on the inner and outer surfaces of the tested concrete sewer pipes. The sewer pipe ID is indicated at the left bottom corner of the images.

Inner surface

Smooth — R700-1996-A-2

Exposed granulates — E300/450-1926-TH-3

Porous mortar between granulates — E400/600-1924-TH-4

Deposits - Dark coloured bands — E400/600-1924-TH-2

Outer surface

Smooth — E300/450-1926-TH-5

Rough — E400/600-1924-A-4

Exposed granulates — E400/600-1924-A-1

Excavation damage — R400-1924-A-2

visible and/or have fallen off. The surface class *Porous mortar between granulates* has similar features to those of the *Exposed granulates* class, but, in addition, the mortar between the larger granulates is porous and has a low apparent cohesion. The *Deposits - Dark coloured bands* class shows remaining material deposits that originate from the varying wastewater level. The surface class *Rough* indicates the occurrence of limited chemical attack, whereby the thin outer mortar layer is still present. Finally, the *Excavation damage* class refers to the condition whereby relatively large parts of the sewer pipe have been scraped off or broken off during their excavation.

2.2.2. Residual alkalinity

The residual alkalinity of the used sewer pipes was determined by means of a phenolphthalein test performed on a representative cross-section obtained after breaking the pipe specimen in two pieces, in accordance with the RILEM procedure described in RILEM TC 56-MHM [45], see also Gu et al. [12] and Oualit et al. [22]. A 1%-phenolphthalein solution was used as a pH-indicator to identify the base-acid transition zones in the concrete cross-sections [46]. The solution colours pink to magenta for moderately alkaline environments with a pH in the range of $9.2 < pH \leq 10$, it colours magenta for highly alkaline environments with a pH > 10, and remains colourless

for slightly alkaline to acidic environments with a pH ≤ 9.2. Naturally, healthy concrete is highly alkaline with a pH-value above 12.5–13, which is caused by the dissolution of solid calcium hydroxide in the pore solution [25,46,47]. However, concrete may experience a decrease in pH-value due to chemo-mechanical degradation processes, such as carbonation [9,19,25,45,47] and biogenic sulphide corrosion [9,11, 48]. In specific, for a fully carbonated concrete material the pH-value commonly ranges between 8.3 and 9, while for biogenic sulphide corrosion it lies between 1 and 3. The spatial transition zone between alkaline and non-alkaline concrete typically is minor in the case of biogenic sulphide corrosion, while for carbonation it can be somewhat larger [16,21,25,40,46]. Accordingly, for biogenic sulphide corrosion the error made in measuring the corrosion depth commonly remains acceptably small when the size of a spatial transition zone is left out of consideration. Although for carbonation the corrosion depth may be slightly underestimated when the contribution related to the pH variation in the spatial transition zone is ignored [25,46,49], this simplification is regularly adopted in the literature [45,50] and also will be used in the present work.

The cross-sectional profile of residual alkalinity and the corresponding thicknesses of the deteriorated layers at the inside and outside of the pipe were measured from photographs of the sprayed cross-sections,
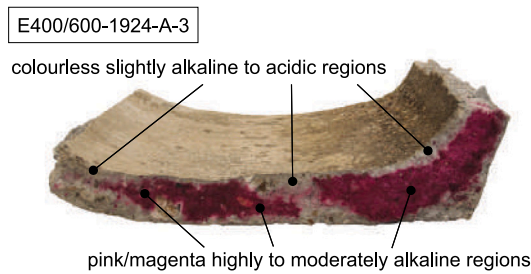
Fig. 2. Residual alkalinity in concrete sewer pipe E400/600-1924-A-3. The pipe cross-section was sprayed with a 1%-phenolphthalein solution, whereby the highly to moderately alkaline regions (pH > 9.2) correspond to the parts for which the solution turns pink/magenta, and the slightly alkaline to acidic regions (pH ≤ 9.2) to the parts for which the solution remains colourless. The photograph was taken 24 h after the phenolphthalein solution was applied. (For interpretation of the references to colour in this figure legend, the reader is referred to the web version of this article.)

Fig. 3. Half cross-section of (a) a round sewer pipe with a flat bottom (dotted line) and without a flat bottom (solid line), and (b) an egg-shaped sewer pipe. The letters *a-t* indicate the 20 locations at which the wall thickness and the thickness of the corrosion layer at the inside and outside of the sewer pipe were measured from a photograph of a cross-section sprayed with the phenolphthalein solution. The regions indicated by the light grey and dark grey colours distinguish 4 cross-sectional areas within which the measured thickness of the corrosion layer was averaged.

which were taken after a 24 h exposure to the phenolphthalein solution. Fig. 2 shows an example of a cross-section sprayed with the phenolph-thalein solution. The highly to moderately alkaline regions (pH > 9.2) correspond to the parts in which the solution turns pink/magenta, and the slightly alkaline to acidic regions (pH ≤ 9.2) to the parts in which the solution remains colourless. From the discolouration profiles, the thicknesses of the deteriorated layers at the inside and outside of the pipe were measured at 20 equidistant locations along one vertical half of the pipe cross-section, as indicated by the letters *a* to *t* in Fig. 3. The average, minimum and maximum thickness profiles of the deterioration layers were subsequently determined per sewer pipe type. Further, the average thicknesses of the deterioration layers were computed per age category, whereby a total number of three age categories was considered, in correspondence with the three decades in which the used sewer pipes were installed, i.e., 1920s, 1950s, 1990s, see Table 1. The thicknesses of the deteriorated layers were subsequently averaged (i) within 4 distinct areas of the sewer pipe cross-section, as indicated in Fig. 3 for the round and egg-shaped pipes, and (ii) over the complete half cross-section of the pipes. Each of the 4 areas includes 5 measurement locations, namely *a* to *e* in area 1, *f* to *j* in area 2, *k* to *o* in area 3 and *p* to *t* in area 4. Note that the measured thickness of a deteriorated layer is somewhat underestimated if spallation of (chemically affected) mortar and/or granulates has occurred during service/excavation of the pipe.

2.2.3. X-ray diffraction analyses

X-ray diffraction (XRD) analyses were carried out to identify char-acteristic chemical compounds from crystallographic structures present in the concrete material of used sewer pipes, which may provide more insight into the chemical attack the pipes have experienced. The XRD analyses were performed on small test samples cut from the used sewer pipes, in conformity with the procedures adopted in Gu et al. [12],Davis et al. [17] and Gutberlet et al. [40]. For each sewer pipe type, one sewer pipe specimen was selected randomly. A core sample was drilled from the top-half of this pipe specimen, and subsequently carefully splitted to obtain small test samples from the inside, mid-thickness and outside of the pipe specimen. These samples were next grinded to fine powder, after which the XRD analyses were carried out by using a Bruker D4 Endeavor operating at 40 kV and 40 mA with Co-Kα radiation. The diffraction data was obtained over an angle 2θ ranging from 10° to 90°, with steps of 0.02° of a duration of 1.5 s.

2.3. Measurement of material properties

The elastic and fracture properties of the concrete material of the new and used sewer pipes were measured by subjecting material samples to uniaxial compression tests and three-point bending tests.
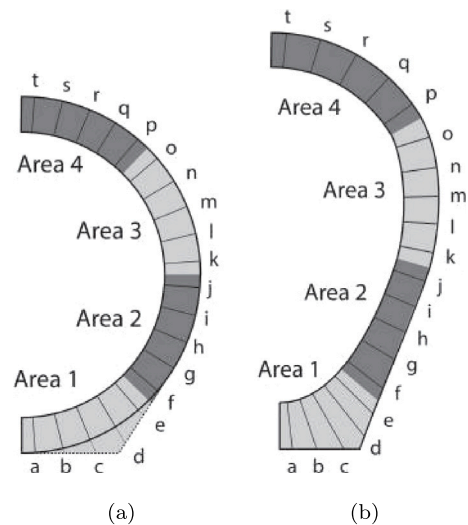
Section 2.3.1 describes the characteristics of the test samples. Sections 2.3.2 and 2.3.3 respectively provide the details of the uniaxial compression test and three-point bending test.

2.3.1. Sample characteristics

The test samples were sawn from the top half of the round sewer pipes and from the circular upper part of the egg-shaped sewer pipes. A schematic representation of the cubic, prismatic and notched beam samples is shown in Fig. 4. The depicted value of the average wall thickness $\bar{t}_w$ is listed in Table 1 for each sewer pipe type. The curvature originating from the circular and egg-shaped sewer pipe geometries was maintained in the test samples, and the sample size was dictated by the wall thickness of the specific sewer pipe type. The Young's modulus and compressive strength were measured in a uniaxial compression test. The measurement of the Young's modulus was performed on 2 to 6 test samples sawn from each pipe specimen, leading to a statistically representative number of 6 to 28 test samples per sewer pipe type. For the measurement of the compressive strength, 6 to 21 test samples were sawn from each pipe specimen, resulting in 23 to 93 test samples per sewer pipe type. The tensile strength and mode I toughness were measured from a three-point bending test, whereby 2 to 6 samples were sawn from each pipe specimen, resulting in a total of 6 to 19 test samples per sewer pipe type.

2.3.2. Young's modulus and compressive strength

The Young's modulus and compressive strength of the concrete sam-ples were determined in accordance with the test procedures presented in NEN-EN 12390-13 [51] and Eurocode NEN-EN 12390-3 [52], respec-tively. The compressive strength was measured by testing the sample in a 4 MN Form+Test Prüfsysteme loading machine. Accordingly, a uniaxial, quasi-static load was applied in a load-controlled fashion via a steel plate and a thin cardboard placed onto the test sample, whereby the loading rate was set equal to 0.6 N/mm²/s, see Fig. 5(a). The compressive strength f_c was calculated by dividing the maximum load applied on the sample by the loading area, and the results where aver-aged over the corresponding number of test samples to determine the average compressive strength per sewer pipe type. The uniaxial test set-up used for measuring the Young's modulus is illustrated in Fig. 5(b).
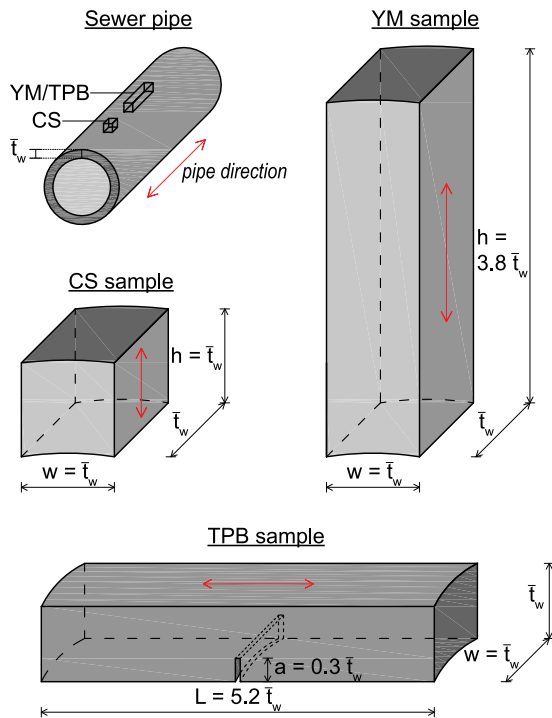
Fig. 4. Samples used in the uniaxial compression tests to obtain the compressive strength (CS sample) and Young's modulus (YM sample), and the notched beam sample used for determining the fracture strength and toughness in the three-point bending tests (TPB sample). The sample dimensions (beam length L, beam width w, beam height h, and notch length a are expressed in terms of the average wall thickness $\bar{t}_w$ of each sewer pipe type, see Table 1 for an overview of the specific values. The notch thickness is equal to 4 mm (not indicated in the figure). The longitudinal direction of the sewer pipe is indicated by a red arrow in the schematic representations of the pipe and test samples. (For interpretation of the references to colour in this figure legend, the reader is referred to the web version of this article.)

The loading was applied onto the specimen via a steel plate using a 250 kN Instron 5985 loading machine. The steel plate was supported by a thin cardboard or soft board sheet in case of a rough specimen surface. The test sample was first loaded for 10 s at a pre-stress equal to $0.125f_c$, which was subsequently increased at a rate of 0.6 N/mm²/s to a value $0.333f_c$. This higher stress value was maintained for 10 s, after which the load was brought back to the original pre-stress of $0.125f_c$ and kept at this level for another 10 s. Next, this load cycle was repeated, during which the Young's modulus E was determined from the incremental load magnitude and the incremental, vertical response of the test sample. The vertical response was taken as the average of the values measured at the front and the back surfaces of the specimen, using Solartron SM3 linear variable displacement transducers (LVDTs). Finally, for each sewer pipe type the Young's modulus was determined as the average over the total number of test specimens.

2.3.3. Tensile strength and mode I toughness

The tensile strength and mode I toughness of the concrete were determined from an experimental-numerical calibration procedure similar to that previously applied for the analysis of the fracture behaviour of oak wood [53]. Accordingly, the response of a notched beam specimen subjected to three-point bending was first captured experimentally, after which Finite Element Method (FEM) analyses were carried out with the commercial software package ABAQUS Standard[1] in which the measured load–displacement behaviour and fracture path of the specimen were closely mimicked. This procedure enables an accurate

_____
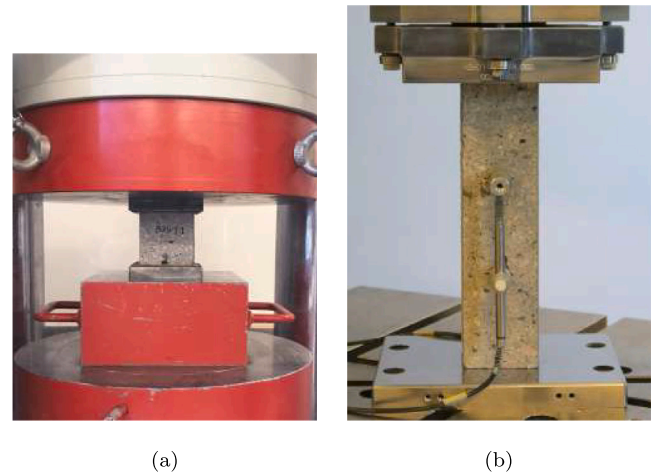[1] Dassault Systems Simulia Corp., Providence, RI, USA.

Fig. 5. Experimental set-up of the (a) uniaxial compression test for determining the concrete compressive strength and (b) uniaxial compression test for determining the Young's modulus. The test sample for measuring the Young's modulus is equipped with an LVDT at the front and back surfaces to determine the relative vertical displacement.

Fig. 6. Experimental set-up of the three-point bending test for determining the concrete tensile strength and mode I toughness. The notched specimen is equipped with an aluminum frame and an LVDT at the front and back sides of the specimen to measure at the point of load application the relative vertical displacement between the top and the centre of the beam.

calibration of the concrete tensile strength and mode I toughness. The experimental set-up of the three-point bending test is shown in Fig. 6, and consists of an Instron 5985 loading machine with a capacity of 250 kN. The notched beam specimen was simply supported across a span width of $4.2\,\bar{t}_w$, with $\bar{t}_w$ the average wall thickness, whereby the supports consisted of thin cardboard on top of a solid steel cylinder. At the mid-span of the sample, the load was quasi-statically applied in a displacement controlled fashion, at an initial rate of 0.01 μm/s. During the macroscopic failure phase of the specimen, the loading rate was increased in a controlled fashion to keep the total test duration reasonable, i.e., between one and two hours. A steel cylinder was used for adequately transferring the load to the specimen. The vertical displacement at the point of load application was measured at the front and back sides of the specimen by Solartron SM3 LVDTs. The displacement transducers were attached onto the surface of the notched beam by means of an aluminium frame and an L-shaped profile, from which the relative displacement between the top and the half height of the beam could be measured, see Fig. 6. The measured load–displacement responses of the samples of each sewer pipe type were used to calibrate "minimum", average and "maximum" values of the tensile strength and mode I toughness from the FEM results, as explained below.

In the FEM analyses, the notched beam is modelled as a two-dimensional, simply-supported structure subjected to plane-stress conditions, as shown in Fig. 7. The geometry of the beam model is discretized using 3-node iso-parametric plane-stress continuum elements with a 1-point Gaussian quadrature. The discrete fracture response is
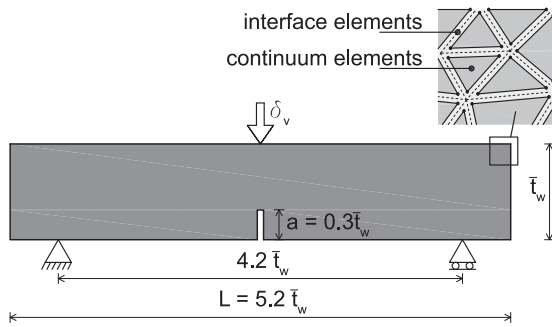
Fig. 7. Geometry and boundary conditions of the two-dimensional plane-stress model of a notched beam subjected to three-point bending. As indicated in the inset, in the FEM model the discrete fracture response is modelled by placing interface elements between adjacent continuum elements.

modelled by placing 4-node interface elements with a 2-point Gaussian quadrature in between all continuum elements, in accordance with the approach originally advocated in Xu and Needleman [54], see the inset of Fig. 7. By choosing a sufficiently small, randomly oriented mesh, this approach allows for the robust simulation of cracks at arbitrary locations and in arbitrary directions, and naturally includes the effects of crack bifurcation, crack branching and crack coalescence, see e.g., Cid Alfaro et al. [55,56]. The interface elements are equipped with the interface damage model presented in Cid Alfaro et al. [57], which has been implemented in ABAQUS as a user-supplied subroutine (commonly referred to as UMAT), and requires the ultimate fracture strength and toughness of the concrete material as essential input parameters. The model further uses a parameter that accounts for possible rate effects in the fracture response, which assists in regularizing fracture responses with complex trajectories towards a physically reliable result, see Cid Alfaro et al. [57] for more details. The interface damage model has demonstrated to realistically and accurately simulate crack initiation and propagation in various materials, such as cementitious materials [37,38], wood [53,58,59], historical paints [60–62], metals [57,63] and fibre-reinforced composites [55,56,64].

The finite element discretization is gradually refined from the supports towards the notch of the beam to closely capture the local stress concentration at the tip of the dominant failure crack developing from the notch. The number of elements used in the beam model is tuned to the actual specimen size, whereby the number of continuum elements varies between 22 000–107 000 and the number of interface elements varies between 33 000–160 000. The Young's modulus used in the continuum elements simulating the elastic bulk response of the concrete material is obtained from the uniaxial compression tests described in Section 2.3.2, see Table 7 for an overview of the measured values. The Poisson's ratio of concrete is taken equal to $\nu = 0.2$, in accordance with the Eurocode EN 1992-1-1 [65].

The elastic stiffness of the interface damage model is given a relatively high value, which guarantees that in the initial, elastic regime of the interface response, the (artificial) interfacial deformations remain small, such that the overall elastic response of the beam specimen is correctly determined by the elastic response of the surrounding continuum elements, see Cid Alfaro et al. [55] for more details. The tensile strength t_1^u and mode I toughness $G_{I,c}$ in the interface damage model are calibrated from the FEM analyses of the three-point bending tests, such that both the experimental load–displacement response and the generated fracture pattern are accurately described. The shear strength t_2^u in the interface damage model is set equal to the tensile strength t_1^u, and the mode II toughness $G_{II,c}$ is set equal to two times the mode I toughness $G_{I,c}$ [66]; these parameters, however, turned out to have a negligible influence on the mode I-dominated fracture responses of the tested samples. The parameters defining the rate-dependency of the

fracture process are set such that the rate-independent limit is closely approached, see Cid Alfaro et al. [55] for more details.

With the FEM models of the test samples, the calibration procedure of the experimental results started by selecting appropriate, initial values for the tensile strength t_1^u and mode I toughness $G_{I,c}$ in the interface damage model. Subsequently, these values were refined in a stepwise fashion from the FEM simulation results using a trial and error procedure, until a close resemblance between the simulated response and the *average* experimental response was achieved. The resemblance between the simulated and average experimental responses was found acceptable when the relative differences between their values for the specimen peak load and between their values for the specimen mode I toughness were less than 4%.

In order to account for the *spread* in the experimental results, two additional FEM simulations were carried out from which the "minimum" and "maximum" values of the concrete tensile strength t_1^u and mode I toughness $G_{I,c}$ were determined. This was done by scaling the calibrated, average response of the three-point bending test such that *both* the specimen peak load and the specimen mode I toughness were respectively decreased and increased by one time their standard deviation as following from the experiments. In Section 3.2.2, it will be demonstrated that the FEM results obtained with the minimum and maximum values of t_1^u and $G_{I,c}$ mimic the overall spread in the experimental specimen responses reasonably well.

3. Experimental results

3.1. Type and degree of deterioration

The type and degree of deterioration of the used sewer pipes are determined by assessing (i) the surface conditions of the pipes, (ii) the residual alkalinity of the pipe cross-sections, and (iii) the presence of characteristic chemical compounds in concrete sewer pipes, applying the methodology presented in Section 2.2. The results of these analyses are respectively summarized in Sections 3.1.1, 3.1.2 and, 3.1.3, and next combined in Section 3.1.4 to identify the main types of chemical degradation.

3.1.1. Sewer pipe surface conditions

The used sewer pipe specimens were subjected to a visual inspection, whereby the classification system presented in Table 3 was applied to identify the corresponding surface conditions at the inner and outer pipe surfaces, see Table 4 for an overview. The surface conditions are analysed at six different locations, namely the top (t), the bottom (b), the left side (l), the right side (r), the bottom-left side (bl) and the bottom-right side (br), whereby the individual locations in the table are separated by a hyphen. It can be observed that the older sewer pipes, which were installed in the 1920s and 1950s, all show deterioration at the inner pipe surface, and in 4 out of 6 cases also at the outer pipe surface. Conversely, the relatively new pipes installed in the 1990s all have smooth surfaces, with occasionally some *Deposits* and *Dark coloured bands* at the inner surface. The surface condition classes related to the most severe degradation, i.e., *Exposed granulates* and *Porous mortar between granulates*, are mainly observed at the right and left sides and at the top of the inner surface of most of the older pipes installed in the 1920s and 1950s. The bottom inside of these sewer pipes shows a lower extent of degradation: only in three cases *Exposed granulates* are detected and in one case this is accompanied by *Porous mortar between granulates*. The *Deposits and Dark coloured bands* are generally located at the bottom-left, bottom and bottom-right sides of the inner surface of the sewer pipes, and are due to the varying wastewater level. During service, three of the four older sewer pipes types characterized by an outer surface condition *Rough* were located below the groundwater level and exposed to mild concentrations of soil pollutants, see Table 2. The excavation damage observed on the outer surface of these 4 sewer pipe types results from the removal of the pipes from the soil, and thus has not affected their performance during service.

Table 4

Surface condition classes per sewer pipe type, as deduced from visual inspections performed on the inner and outer pipe surfaces. The classification is applied to 4 principal locations along the pipe circumference, i.e., the top (t), left side (l), right side (r), bottom (b), and to the intermediate bottom-left (bl) and bottom-right (br) locations, with individual locations being separated by a hyphen. Illustrations of these surface condition classes are presented in Table 3.

ID	Surface condition class inner surface				Surface condition class outer surface			
	Smooth	Exposed granulates	Porous mortar between granulates	Deposits - Dark coloured bands	Smooth	Rough	Exposed granulates	Excavation damage
R400-1924-A		t-l-r-b	t-l-r-b	bl-br	t-l-r-b			t-b
R500-1997-A	t-l-r-b				t-l-r-b			
R700-1996-A	t-l-r-b			bl-br	t-l-r-b			
E300/450-1951-TH		t-l-r-b	t-l-r	bl-br-b		t-l-r-b		t-l-r
E300/450-1926-TH	b	t-l-r	t-l-r	bl-br	t-l-r-b			
E400/600-1951-TH	b	t-l-r		bl-br-b		t-l-r-b		t-b
E400/600-1924-TH	b	t-l-r	t-l-r	bl-br-b	t-l-r-b			
E400/600-1924-A	t-l-r	b				t-l-r	b-r	t
E800/1200–1954-A	l-r-b	t		bl-br-b		t-l-r-b		t-r

3.1.2. Residual alkalinity

The measurement of the residual alkalinity of the cross-sections of the *used* sewer pipes allows to distinguish the *chemically attacked concrete* from the *healthy concrete*, in accordance with the procedure described in Section 2.2.2. The results from the residual alkalinity tests are summarized per sewer pipe type in the contour plots in Fig. 8, whereby the colour range from *white* to *dark red* respectively denotes the transition from *chemically attacked concrete* (pH $\leq$ 9.2) to *healthy concrete* (pH > 9.2). Note that the results of the relatively new sewer pipe type R500-1997-A are omitted, as these are comparable to those of the relatively new sewer pipe type R700-1996-A.

The contour plots are constructed as follows: at the 20 locations a to t indicated in Fig. 3, for each sewer pipe type the *average thickness* and the *minimum* and *maximum thicknesses* of the chemically attacked layer are determined over the corresponding number of pipes listed in Table 1. For the regions falling in between the 20 measurement locations, the thickness values in the contour plot are determined by means of linear interpolation. Using the 4 selected colours *white*, *light red*, *red* and *dark red*, the inset of Fig. 3 shows that the average thickness and thickness extremes of the *chemically attacked concrete* in the contour plot are displayed as follows: white region (minimum thickness), white + light red regions (average thickness) and white + light red + red regions (maximum thickness). In addition, the average thickness and thickness extremes of the *healthy concrete* are displayed as follows: dark red region (minimum thickness), dark red + red regions (average thickness) and dark red + red + light red regions (maximum thickness). Furthermore, Table 5 summarizes the average thicknesses of the chemically attacked concrete layers $\bar{t}_{chem}$ at the inside and outside of the pipe for each of the four distinct areas defined on the sewer pipe cross-section (shown in Fig. 3) and for the complete half cross-section. Note that the values of $\bar{t}_{chem}$ are determined per sewer pipe type (top of the table) and per age category (bottom of the table).

From Fig. 8 and Table 5 it can be concluded that *all* sewer pipes from the 1920s and 1950s show (bio-)chemical attack at the inside and outside. The degree of chemical attack varies per sewer pipe type, and generally is non-uniform along the inner and outer circumferences of the pipes. The relatively old sewer pipe type R400-1924-A from the 1920s clearly shows the largest chemical attack, with substantial corrosion present along the *complete* inner and outer circumferences. Specifically, along the inner circumference a maximum corrosion depth of approximately 23 mm is observed in areas 2 and 3, which corresponds to 43% of the average wall thickness $\bar{t}_w$ of pipe R400-1924-A. In areas 4 (bottom) and 1 (top) the corrosion depth is somewhat smaller and equal to 20.5 mm (= $0.38\bar{t}_w$) and 19.1 mm (= $0.35\bar{t}_w$), respectively. Note that the above values do not account for a possible material spallation. Along the outer circumference of the R400-1924-A pipe, a substantial amount of corrosion can be identified in areas 2, 3 and 4, whereby the corrosion depths are comparable, and approximately equal to 22 mm (= $0.4\bar{t}_w$). Conversely, area 1 located at the bottom of the pipe shows less chemical attack, in correspondence with a corrosion depth of 5.7 mm (= $0.11\bar{t}_w$). In summary, the above results indicate that in areas 2, 3 and 4 almost the entire wall of the R400-1924-A pipes is corroded.

Observe further from Fig. 8 and Table 5 that the other, relatively old sewer pipes from the 1920s and 1950s mostly show non-uniform chemical corrosion in all 4 areas, although the extent is a factor of two or more less than for pipe type R400-1924-A considered above. In contrast, for the relatively new pipes from the 1990s the chemical attack is negligible, both at the inside and outside, which is probably due to the relatively short service life of these pipes. In order to obtain more insight into this aspect, in Figs. 9(a) and 9(b) the average corrosion depth $\bar{t}_{chem}$ at respectively the inner and outer pipe surface (as reported in Table 5) is plotted against the average year of pipe installation per decade, i.e., 1925, 1952 and 1997 for the pipes from the 1920s, 1950s and 1990s, respectively (as indicated by the black solid squares). Here, the error bars for $\bar{t}_{chem}$ correspond to the minimum and maximum corrosion depths measured (as following from Table 5). Further, the dashed line denotes the linear trend obtained after fitting the measured values of the average corrosion depth. The good agreement between the trend lines and the average corrosion depths indicates that the amount of chemical degradation increases approximately linearly over time. A linear increase of the corrosion depth at the inner surface of sewer pipes over their lifetime has also been reported in Wells and Melchers [14]. In this work, the corrosion loss for a variety of concrete sewer pipes near Melbourne, Australia was evaluated, which had been in service for different periods, up to 18 years. From the measurement results, it was concluded that the corrosion rate at the inner pipe surface remains approximately constant with time, provided that the exposure conditions remain more or less the same.

A comparison of the slopes of the trend lines depicted in Figs. 9(a) and (b) illustrates that the rate of chemical attack at the inside of the pipe on average is about 1.3 times higher than at the outside. Observe further that both trend lines intersect the horizontal axis $\bar{t}_{chem} = 0$ close to the year 1997, which indeed implies that for the relatively new sewer pipes installed in 1997 no significant chemical degradation can be expected, see also Table 5. Finally, the relatively large error bars in Figs. 9(a) and (b) indicate a substantial variability in the mean corrosion depth over the different types of sewer pipes, from which it is concluded that the linearity of the fitted trendline should be treated with some caution. Essentially, a unique, explicit relation between the age of the pipe and the degree of chemical degradation may not be deduced from the measurement data; as indicated by the size of the error bars, the specific local environmental conditions and the geometrical and material characteristics of a pipe also have a substantial influence on the time development of chemical corrosion.
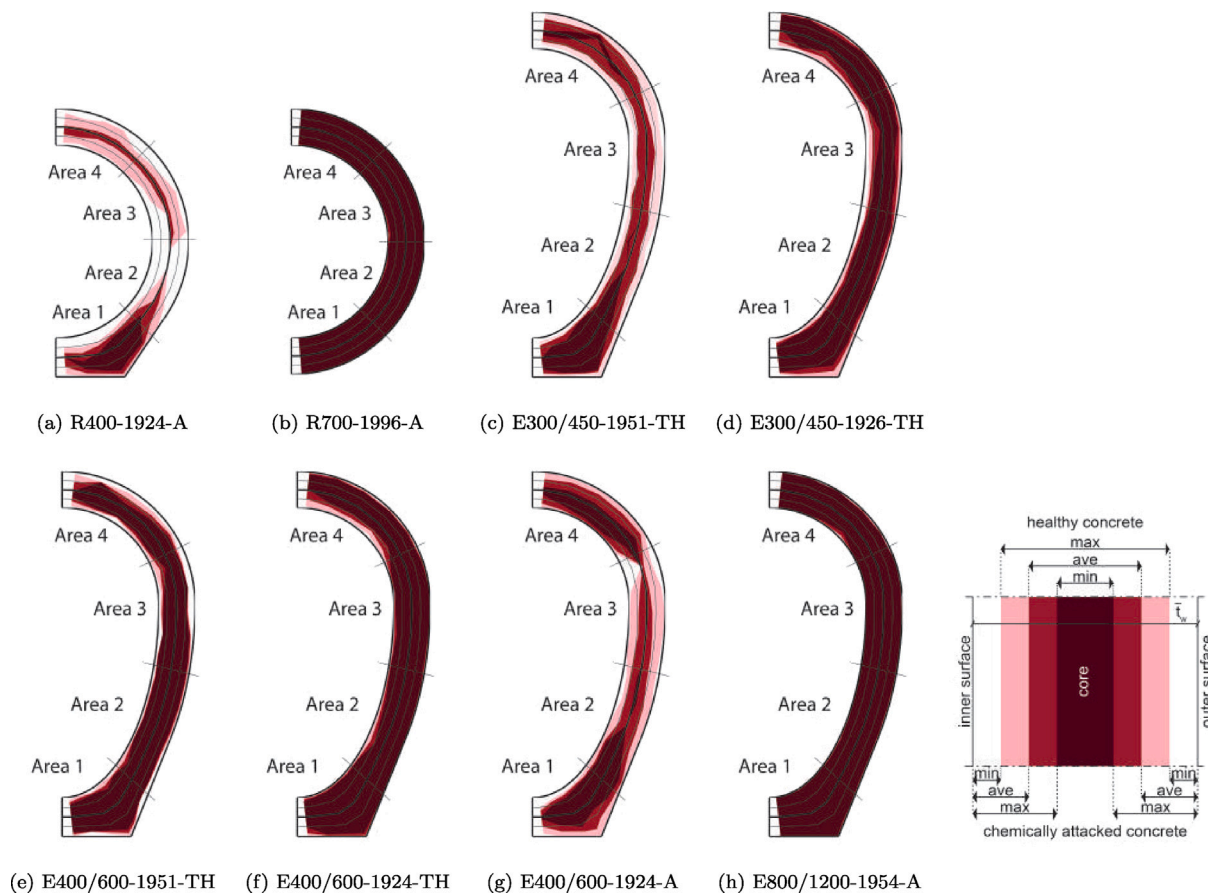
Fig. 8. Residual alkalinity of concrete measured on the cross-section of various types of used sewer pipes by means of phenolphthalein tests. The transitions from the minimum, average and maximum thickness of the healthy concrete to respectively the maximum, average and minimum thickness of the chemically attacked layer are indicated in the colour scheme shown in the inset at the bottom right. (For interpretation of the references to colour in this figure legend, the reader is referred to the web version of this article.)

Table 5
Average corrosion depth $\bar{t}_{chem}$ (in mm) at the inside and outside of sewer pipes for four distinct areas on the sewer pipe cross-section (as designated in Fig. 3) and for the complete half cross-section. The values are presented per sewer pipe type (top of the table) and per age category (bottom of the table, considering only the used pipes).

ID	Inside					Outside				
	Area 1 [mm]	Area 2 [mm]	Area 3 [mm]	Area 4 [mm]	Half cross. [mm]	Area 1 [mm]	Area 2 [mm]	Area 3 [mm]	Area 4 [mm]	Half cross. [mm]
R400-1924-A	19.1	22.1	23.4	17.5	20.5	5.7	21.3	21.6	22.4	17.7
R500-1997-A	0.0	0.0	0.0	0.0	0.0	0.1	0.8	0.0	0.0	0.2
R700-1996-A	0.5	0.8	1.5	1.1	1.0	0.0	0.0	0.0	0.0	0.0
E300/450-1951-TH	8.8	11.1	12.0	11.9	10.9	6.7	11.7	16.5	9.4	11.1
E300/450-1926-TH	6.4	7.6	10.3	7.2	7.9	6.2	2.4	3.3	1.0	3.2
E400/600-1951-TH	8.6	5.8	8.2	8.7	7.8	7.5	4.4	8.5	13.2	8.4
E400/600-1924-TH	3.3	5.1	2.3	11.9	5.6	2.2	0.2	0.0	1.6	1.1
E400/600-1924-A	14.6	12.9	19.2	4.2	12.7	12.8	11.5	20.9	8.3	13.4
E800/1200–1954-A	2.3	3.3	1.3	2.6	2.4	1.0	1.8	0.9	1.3	1.3
Group used 1990s					0.5					0.1
Group used 1950s					7.0					6.8
Group used 1920s					11.7					8.8

3.1.3. X-ray diffraction analyses

XRD analyses were carried out to identify characteristic chemical compounds in the concrete material of used sewer pipes, from which a specific type of chemical attack may be identified. Fig. 10 shows two representative diffraction patterns, whereby the position and the intensity (i.e., the counts) of the peaks are determined for crystalline structures present in the sample. Observe from Fig. 10(a) that the diffraction pattern of the sample located at the inside of sewer pipe E400/600-1951-TH-2 shows traces of quartz and gypsum and that the sample located at the outside of sewer pipe E400/600-1924-A-1 (Fig. 10(b)) reveals the presence of quartz and calcite.

The results of all diffraction patterns are grouped per sewer pipe type, as listed in Table 6. The outcome is divided into three categories, i.e., *inside*, *mid-thickness* and *outside*, which refer to the locations at which the small test samples were taken from the sewer pipe specimens. Table 6 shows that the test samples contained quartz (silicon dioxide, $S_i(OH)_2$), and often various feldspars. These minerals indeed are largely present in the sand and aggregate constituents of concrete. In addition, calcium hydroxide ($Ca(OH)_2$), gypsum ($CaSO_4 \cdot 2H_2O$) and calcite ($CaCO_3$) were found, which respectively indicate the presence of healthy (alkaline) concrete, biogenic sulphide corrosion and carbonation [9,11,16,19,25,45–48]. Calcium hydroxide is present only at the
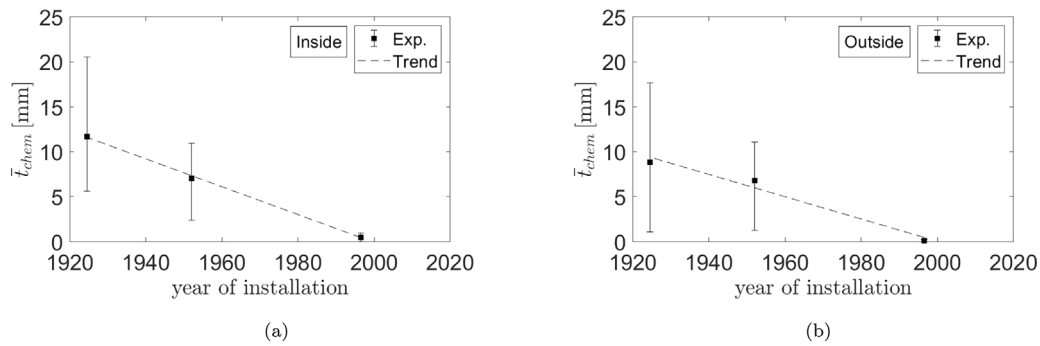
Fig. 9. Average corrosion depth $\bar{t}_{chem}$ as a function of the year of pipe installation, measured at the (a) inside and (b) outside of the sewer pipes. The black solid squares indicate the measured average corrosion depths, with the error bars reflecting the minimum and maximum experimental values. The dashed line represents the linear trend obtained after fitting the measured average corrosion depths.
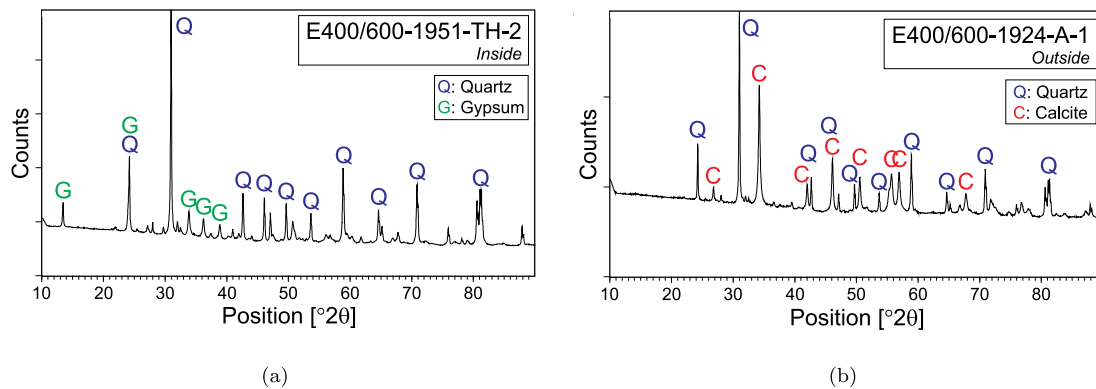

Fig. 10. XRD patterns for sewer pipes (a) E400/600-1951-TH-2 (at the inside of the pipe) and (b) E400/600-1924-A-1 (at the outside of the pipe). The peaks corresponding to quartz, gypsum and calcite are indicated by a blue "Q", a green "G" and a red "C", respectively. (For interpretation of the references to colour in this figure legend, the reader is referred to the web version of this article.)

Table 6
Chemical compounds found in the used sewer pipes by means of XRD analyses, as indicated by an "x". Three different sample locations were considered, i.e., at the *inside*, *mid-thickness*, and *outside* of the sewer pipes.

ID	Inside					Mid-thickness					Outside				
	Quartz	Feldspar	Ca. Hydr.	Gypsum	Calcite	Quartz	Feldspar	Ca. Hydr.	Gypsum	Calcite	Quartz	Feldspar	Ca. Hydr.	Gypsum	Calcite
R400-1924-A	x	x				x	x			x	x				x
R500-1997-A	x				x	x	x				x	x			x
R700-1996-A	x					x	x	x			x	x			x
E300/450-1951-TH	x	x				x	x			x	x				x
E300/450-1926-TH	x	x				x		x			x	x	x		x
E400/600-1951-TH	x			x		x	x			x	x				x
E400/600-1924-TH	x	x		x		x		x			x				x
E400/600-1924-A	x			x		x				x	x				x
E800/1200–1954-A	x	x		x		x	x	x			x				x

mid-thickness of some of the sewer pipe types; this suggests that in the other pipe specimens calcium hydroxide dissolution took place, thereby providing calcium ions necessary for gypsum and calcite formation. Indeed, traces of gypsum were found at the inside of the E400/600-1951-TH and E400/600-1924-TH sewer pipes. Furthermore, calcite was found at the outside of all 9 sewer pipe types, and also at the inside and mid-thickness of some of the sewer pipes.

3.1.4. Identification of type and degree of chemical attack

The type and degree of chemical attack of the used sewer pipes can be identified by systematically combining the above measurement results. The residual alkalinity profiles depicted in Fig. 8 show that chemical attack mainly took place at the inside and outside of the pipes; accordingly, the type of chemical attack will be successively identified at these two locations. The focus hereby lies on the used sewer pipes installed in the 1920s and 1950s, since for the pipes installed in the 1990s the amount of chemical attack is negligible, see Figs. 8(b) and 9.

- *Inside of sewer pipes*: From the results of the phenolphthalein tests illustrated in Fig. 8, it becomes clear that large parts at the inside of the pipes installed in the 1920s and 1950s are slightly alkaline to acidic with a pH $\leq$ 9.2, which denotes a certain type of chemical attack. Further, the XRD analyses show the presence of gypsum at the inner surface of some of the pipe specimens, and generally indicate the dissolution of calcium hydroxide that provides the calcium ions necessary for gypsum formation, see Table 6. Gypsum is a highly porous material that easily spalls off if a critical thickness is achieved [16,17], or simply may be washed off by the wastewater. This explains why the inner surfaces of most of the relatively old sewer pipes show substantial signs of deterioration by *Exposed granulates* and *Porous mortar between granulates*, see Table 4, and that gypsum was not found in all older sewer pipes, see Table 6. The formation of gypsum at the inner pipe surface typically is caused by *biogenic sulphide*

corrosion. In this process, bacteria present in the thin moisture layer along the inner pipe surface convert the dissolved ionic species of the hydrogen sulphide gas released by the wastewater into sulphuric acid, which diffuses into the concrete and reacts with the available calcium hydroxide and calcium silicate hydrate to form gypsum [11,12,15,16,21]. The porous gypsum layer formed at the inner pipe surface not only has inferior mechanical properties compared to the original cement paste [12,17,22,23], its expansive nature may also result in critical tensile stresses that initiate micro-cracks and lead to the development of macroscopic damage [16]. The consequent reduction of the undamaged, healthy concrete material across the pipe wall can have serious implications for the load bearing capacity of the pipe: a recent experimental-numerical study on different sewer pipe types presented in Scheperboer et al. [37] showed that a reduction of 20% of the concrete wall thickness can already diminish the load bearing capacity of the pipe by 40%. Due to a broad availability of nutrients for bacteria caused by a varying wastewater level, and the upward flow direction of the hydrogen sulphide gas released by the wastewater, biogenic sulphide corrosion is most severe at, respectively, the tidal zone [17,43,67] and the crown of the sewer pipe [43,68,69]. Note from Fig. 8 that these two inner surface locations indeed appear as the severely corroded areas 2 and 3 (tidal zone) and area 4 (crown).

- *Outside of sewer pipes:* The results of the phenolphthalein tests depicted in Fig. 8 illustrate that for several pipes large parts at the outer surfaces are slightly alkaline to acidic with a pH ≤ 9.2, and thus are chemically affected. In addition, the XRD analyses indicate the presence of calcite at the outer surface of all sewer pipe types, see Table 6, which, in combination with the observed surface conditions *Smooth* and *Rough* listed in Table 3, suggest chemical attack by *carbonation*. Carbonation is due to the diffusion of carbon dioxide naturally present in soil towards the outer surface of concrete sewer pipes, at which it can react with hydrated cement in the presence of moisture [22,25]. Although this process may cause the strength and stiffness properties to increase as a result of a decrease in porosity and structural changes in calcium silicate hydrates, this positive effect can be mitigated, or even reversed, in a negative effect by carbonation shrinkage and consequent crack formation [25]. The complex combination of these two mechanisms essentially makes it difficult to a priori assess the influence of carbonation on the mechanical and functional properties of the sewer pipe, as a result of which its effect currently is a topic of debate in the concrete engineering community [25]. Moreover, from the pipe surface conditions presented in Table 3, it may be deduced that the net result of carbonation is less harmful to the integrity of the sewer system compared to chemical attack by biogenic sulphide corrosion at the inner pipe surface. This conclusion is further supported by the fact that only mild concentrations of soil pollutants that potentially stimulate outer pipe corrosion were found at the *in-situ* locations of the sewer pipes, such as mineral oil [70], see Table 2 and the discussion in Section 2.1.2.

3.2. Material properties

The material properties of the concrete sewer pipes were determined from the mechanical tests described in Section 2.3. The measurement results for the Young's modulus and compressive strength are discussed in Section 3.2.1, and the results for the tensile strength and mode I toughness are treated in Section 3.2.2.

Table 7

Average experimental values of the concrete Young's modulus $\bar{E}$ and compressive strength $\bar{f}_c$ (in N/mm^2), and the corresponding standard deviations S_E and S_{f_c}, as obtained from the uniaxial compression tests shown in Fig. 5. The measured values are presented per sewer pipe type (top of the table) and per age category (bottom of the table).

ID	$\bar{E}$ [N/mm^2]	S_E [N/mm^2]	$\bar{f}_c$ [N/mm^2]	S_{f_c} [N/mm^2]
R400-2015-new	48 697	2 460	85.1	8.9
R400-1924-A	31 338	6 386	44.6	12.1
R500-2015-new	44 413	3 136	80.0	10.8
R500-1997-A	52 193	4 705	67.7	9.1
R700-1996-A	46 412	2 172	64.5	7.9
E300/450-1951-TH	41 916	6 911	46.7	12.9
E300/450-1926-TH	43 911	5 349	45.1	14.7
E400/600-2015-new	47 067	1 385	85.5	5.7
E400/600-1951-TH	37 910	6 226	49.8	7.8
E400/600-1924-TH	39 293	4 157	61.1	13.1
E400/600-1924-A	42 478	3 082	50.8	9.4
E800/1200–1954-A	45 746	2 204	83.1	11.2
Group new 2015	46 259	3 077	83.6	8.7
Group used 1990s	48 048	3 800	65.6	8.4
Group used 1950s	41 620	6 625	53.4	17.3
Group used 1920s	38 738	6 968	49.9	14.3

3.2.1. Young's modulus and compressive strength

Table 7 lists the average value and corresponding standard deviation of the Young's modulus ($\bar{E}$, S_E) and compressive strength ($\bar{f}_c$, S_{f_c}), as obtained from the uniaxial compression tests. The measurement results are averaged per sewer pipe type (top of the table) and per age category (bottom of the table). The values listed for the standard deviation of the Young's modulus and compressive strength indicate that the spread of these material parameters for each sewer pipe type and for each age category is significant, which may be ascribed to differences in the concrete composition and *in-situ* conditions of individual sewer pipes, as well as the material heterogeneity of concrete within a single sewer pipe. The measured values are comparable to those reported in other experimental works, see Hu et al. [71],Fan et al. [72] for the Young's modulus and Davis et al. [17],Oualit et al. [22],Ortega et al. [73] for the compressive strength. Observe further from the table that the average values of the two material parameters tend to decrease with age. This aspect is revealed in more detail in Figs. 11(a) and (b), which respectively illustrate the average Young's modulus and compressive strength of the concrete material as a function of the year of installation of the corresponding sewer pipes. Here, the linear trends (dashed line) follow from fitting the average measurement values, and the spread in measurement results designated by the errors bars corresponds to one time the standard deviation. The decrease of the concrete Young's modulus with age is rather mild, and in fact can be assessed as negligible when considering the substantial spread in the experimental values. Conversely, the decrease of the average concrete compressive strength with age is significant: the measured concrete strength of the sewer pipes from the 1920s equals $\bar{f}_c$ = 49.9 N/mm^2, and is a factor of 1.7 lower than the measured concrete strength $\bar{f}_c$ = 83.6 N/mm^2 of the new sewer pipes from 2015. The linear time decrease of the average compressive strength probably mostly is due to the linear time increase of the inner corrosion layer, as induced by the process of biogenic sulphide corrosion, see Fig. 9(a). A decrease of the concrete compressive strength due to biogenic sulphide corrosion has also been reported in other works [12,16,17,22,23], and may be attributed to the increase in material porosity (i.e., damage) and the relatively low strength properties of gypsum.

3.2.2. Tensile strength and mode I toughness

The tensile strength and mode I toughness were calibrated from the failure response of concrete specimens subjected to three-point bending, as depicted in Fig. 12(a) and (b) for samples taken from new (E400/600-new) and old (E400/600-1924-A) sewer pipes. The
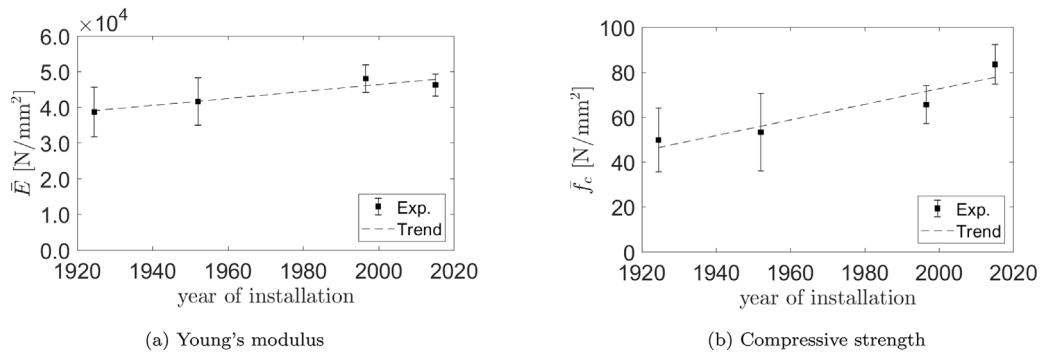
Fig. 11. Concrete material properties versus the year of installation of the corresponding group of sewer pipes. (a) Average Young's modulus $\bar{E}$, and (b) average compressive strength $\bar{f}_c$. The black solid squares indicate the average experimental values, with the error bars representing one time the standard deviation of the measurement results. The dashed line represents the linear trend obtained after fitting the average experimental values.
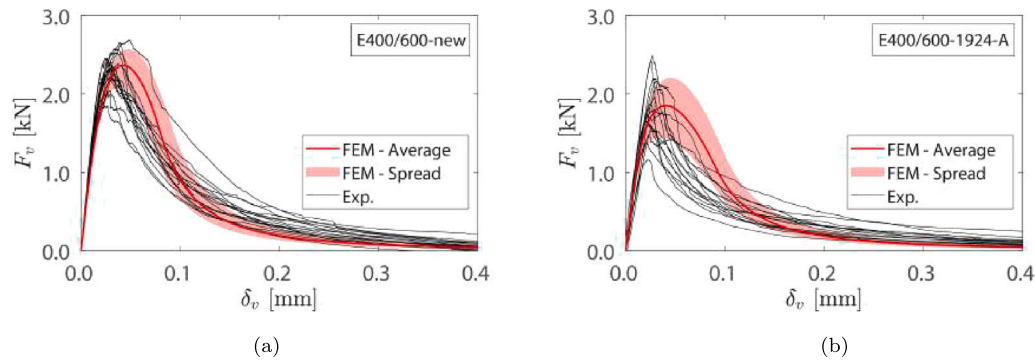

Fig. 12. Load–displacement response of the notched beam specimens under three-point bending, showing the vertical load F_v as a function of the load point deflection δ_v at the mid-span of the beam. (a) E400/600-new pipe, and (b) E400/600-1924-A pipe. The experimental responses are shown by the black lines, the calibrated average response is indicated by the thick red line, and the corresponding spread is represented by the red hatched area. The outer limits of the spread have been determined in accordance with one time the standard deviation of the peak load and mode I toughness measured for the specimen. Table 8 lists the average values of the concrete tensile strength and mode I toughness used for computing the average specimen response, and their maximum and minimum values used for computing the outer limits of the spread. (For interpretation of the references to colour in this figure legend, the reader is referred to the web version of this article.)

experimental responses of the various samples are shown by the black lines, the average response as obtained from the calibration procedure is indicated by the thick red line, and the spread is represented by the red hatched area; Table 8 lists the average values for the concrete tensile strength $\bar{t}_1^u$ and mode I toughness $\bar{G}_{I,c}$ used for computing the average response, and the minimum and maximum values ($t_{1;min}^u$, $t_{1;max}^u$) and ($G_{I,c;min}$, $G_{I,c;max}$) used for computing the outer limits of the spread. It can be observed that the spread in the numerical simulations captures the variation in the experimental responses reasonably well. The response initially is elastic, whereby the load point deflection δ_v increases proportionally with the applied load F_v. After reaching the maximum load, softening occurs whereby the load point deflection increases under a continuous decrease in the applied load, up to the stage where the load becomes zero and the specimen fails completely. For all concrete test specimens, the catastrophic failure crack characterizing the softening branch developed approximately vertically, from the central notch towards the upper specimen boundary, with a local occurrence of small oscillations due to the presence of material heterogeneities (i.e., aggregates), see Fig. 13(a) for the E400/600-new sewer pipe and the E400/600-1924-A sewer pipe. The FEM simulation used for the calibration of the fracture parameters shows a comparable crack trajectory, see Fig. 13(b), whereby local crack oscillations remain absent due to the assumption of a homogeneous material.

The calibrated values for the tensile strength and mode I toughness summarized in Table 8 are comparable to the concrete tensile strength [22,71] and mode I toughness [74] reported in other works. The fracture parameters are presented for each sewer pipe type (top of the table), together with the average values for each age category

(bottom of the table). As observed for the Young's modulus and compressive strength, the spread in values of the tensile strength and mode I toughness is considerable for each sewer pipe type and age category, due to variations in material composition and the *in-situ* conditions of the sewer pipes, as well as the material heterogeneity of concrete within a single sewer pipe. The change of the fracture parameters with age is further clarified in Fig. 14, showing that the average tensile strength $\bar{t}_1^u$ substantially decreases with age, while the average mode I toughness $\bar{G}_{I,c}$ remains almost constant. The relative decrease with age for the concrete tensile strength is somewhat less than for the compressive strength illustrated in Fig. 11(b), and over a period of almost 100 years corresponds to a factor of about 1.5, as computed from the average concrete tensile strengths measured for the new sewer pipes from 2015 ($\bar{t}_1^u = 4.2$ N/mm^2) and the old pipes from the 1920s ($\bar{t}_1^u = 2.9$ N/mm^2). Again, the origin of this decrease lies in the process of biogenic sulphide corrosion, and contributes to the fact that the ultimate bearing strength of the old sewer pipes from the 1920s in principle can be more than a factor of two lower than that of the new sewer pipes from 2015, see Luimes et al. [38] for more details on this aspect.

It is finally noted that the measured values listed in Tables 7 and 8 for the Young's modulus, compressive strength, tensile strength, and mode I toughness of new and aged concrete may serve as input for detailed FEM analyses on the mechanical failure behaviour of new and aged sewer pipes, such as respectively performed in Scheperboer et al. [37] and Luimes et al. [38].

4. Conclusions and practical recommendations

The chemo-mechanical degradation of unreinforced concrete sewer pipes applied in domestic service locations has been assessed through a
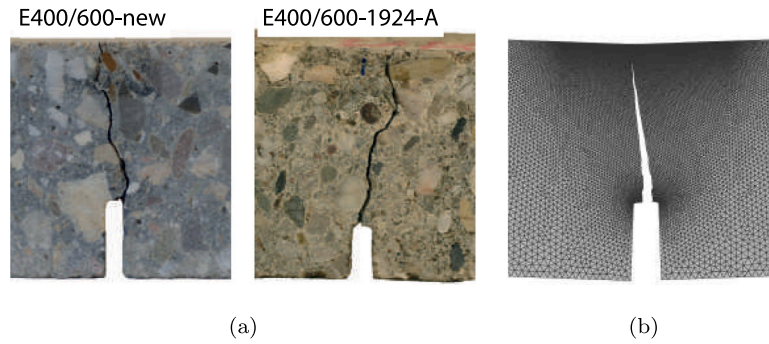
E400/600-new   E400/600-1924-A

(a)   (b)

Fig. 13. Fracture path leading to failure of the three-point bending specimen. (a) Specimens taken from the E400/600-new (left) and E400/600-1924-A (right) sewer pipes, and (b) FEM result representative of a specimen taken from the R400-new sewer pipe, whereby the deformations are magnified by a factor of 10 for clarification.
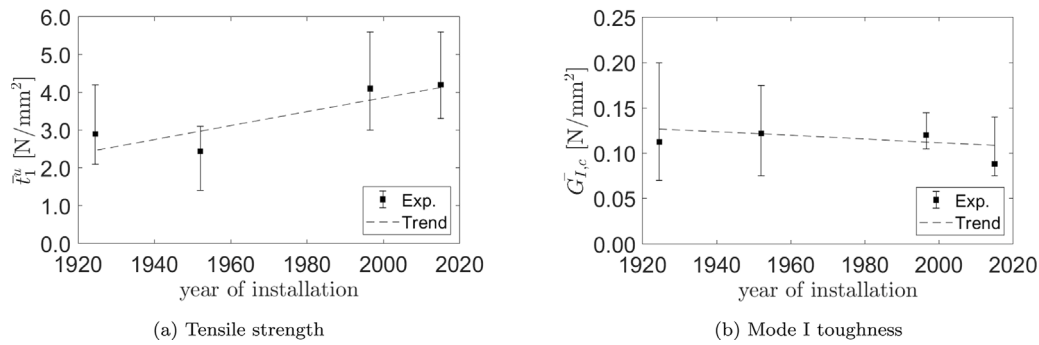

(a) Tensile strength   (b) Mode I toughness

Fig. 14. Concrete material properties versus the year of installation of the corresponding group of sewer pipes. (a) Average tensile strength $\bar{t}_u^1$, and (b) average mode I toughness $\bar{G}_{I,c}$. The black solid squares indicate the average experimental values, with the error bars representing the spread in measurement results. The dashed line represents the linear trend obtained after fitting the average experimental values.

Table 8

Average experimental values of the concrete tensile strength $\bar{t}_1^u$ (in N/mm²) and mode I toughness $\bar{G}_{I,c}$ (in N/mm), and the corresponding minimum ($t_{1;min}^u$, $G_{I,c;min}$) and maximum ($t_{1;max}^u$, $G_{I,c;max}$) values, as obtained from the three-point bending tests shown in Fig. 6. The measured values are presented per sewer pipe type (top of the table) and age category (bottom of the table).

ID	$t_{1;min}^u$ [N/mm²]	$\bar{t}_1^u$ [N/mm²]	$t_{1;max}^u$ [N/mm²]	$G_{I,c;min}$ [N/mm]	$\bar{G}_{I,c}$ [N/mm]	$G_{I,c;max}$ [N/mm]
R400-new	4.1	4.6	5.6	0.075	0.080	0.105
R400-1924-A	2.3	2.9	3.7	0.070	0.090	0.125
R500-new	3.3	3.9	4.7	0.075	0.080	0.095
R500-1997-A	4.8	5.0	5.6	0.105	0.115	0.135
R700-1996-A	3.0	3.2	3.6	0.105	0.125	0.145
E300/450-1951-TH	1.6	2.1	2.6	0.085	0.115	0.140
E300/450-1926-TH	2.1	2.8	3.4	0.110	0.150	0.200
E400/600-new	3.7	4.1	4.5	0.095	0.105	0.140
E400/600-1951-TH	1.4	2.2	2.9	0.075	0.100	0.140
E400/600-1924-TH	2.1	3.1	4.2	0.090	0.120	0.160
E400/600-1924-A	2.1	2.8	3.4	0.075	0.090	0.120
E800/1200–1954-A	3.0	3.0	3.1	0.125	0.150	0.175
Group new 2015	3.3	4.2	5.6	0.075	0.088	0.140
Group used 1990s	3.0	4.1	5.6	0.105	0.120	0.145
Group used 1950s	1.4	2.4	3.1	0.075	0.122	0.175
Group used 1920s	2.1	2.9	4.2	0.070	0.113	0.200

systematic, integrated experimental approach, considering 18 new and 35 used sewer pipes. The characteristics and environmental conditions of the sewer pipes have been reported, and data obtained from surface condition classification, residual alkalinity tests and XRD analyses have been combined to identify the type and degree of chemical attack of the used sewer pipes. Concrete material properties have been determined by material tests on sewer pipe samples, providing quantitative insight into the age dependency of the Young's modulus, compressive strength, tensile strength and mode I toughness. The main conclusions and practical recommendations of this work are summarized below.

- Large parts of the inside of the relatively old pipes installed in the 1920s and 1950s are slightly alkaline to acidic, and suggest

chemical attack by biogenic sulphide corrosion, see Fig. 8. This process leads to the formation of gypsum, which is a highly porous material that easily spalls off if a critical thickness is achieved, or simply may be washed off by the wastewater. Accordingly, almost all of the relatively old sewer pipes show a substantial deterioration at the inside, in the form of *exposed granulates* and *porous mortar between granulates*. The outside of most sewer pipes has been affected by the process of carbonation, which is characterized by the presence of calcite and provides the pipes with a smooth to rough outer surface. The net result of carbonation on the integrity of sewer pipes is still a topic of debate in the concrete engineering community, but may be

assumed to be less harmful than the effect by biogenic sulphide corrosion.

- The relatively new sewer pipes from the 1990s show almost no signs of chemical attack, see Figs. 8(b) and 9 and Table 5. This implies that, during the first 25 years after sewer pipe installation in domestic service locations, the frequency and intensity of maintenance inspections on pipe degradation can be kept limited.
- The time development of corrosion by biogenic sulphide corrosion (at the inside of the pipe) and carbonation (at the outside of the pipe) on average follows a linear trend, see Figs. 9(a) and (b), respectively. The corrosion rate for biogenic sulphide corrosion appears to be about 1.3 times larger than for carbonation, whereby the combination of the two processes has caused that for one of the old pipes from 1924 almost the entire pipe wall has corroded, see Fig. 8(a). It is emphasized, however, that a unique, explicit relation between the age of the pipe and the degree of chemical attack may not be deduced from the results in Fig. 9; as indicated by the size of the error bars, the specific local environmental conditions and the geometrical and material characteristics of the pipe also have a significant influence on the time development of chemical corrosion.
- Chemical attack by biogenic sulphide corrosion turned out to be most severe in the tidal zone and the crown of the sewer pipe, as can be observed from areas 2 and 3 (tidal zone) and area 4 (crown) in Fig. 8. This can be explained from the broad availability of nutrients for bacteria in the tidal zone under a varying wastewater level, and the upward flow to the crown of the hydrogen sulphide gas released by the wastewater.
- Material tests performed on samples taken from the sewer pipes indicated that the mechanical properties of the concrete may significantly depend on the age of the sewer pipe. In particular, the average compressive strength and tensile strength decrease approximately linearly with the age of the pipe, see Figs. 11(b) and 14(a), in correspondence with a respective reduction of a factor of 1.7 and 1.5 over a period of almost 100 years (i.e., from the 1920s to 2015). Conversely, the age dependency of the concrete Young's modulus and mode I toughness is mild to negligible, see Figs. 11(a) and 14(b). The reduction in concrete compressive and tensile strengths with age mostly may be attributed to the process of biogenic sulphide corrosion, as characterized by an increase in material porosity (i.e., damage) and the relatively low strength properties of gypsum.
- The results presented in this work have been established by means of an integrated experimental approach, which clearly demonstrates that visual inspection alone is not sufficient for assessing the physical condition and structural integrity of *in-situ* sewer pipes. This conclusion is in agreement with other studies [2,3,6].
- As recently pointed out in Scheperboer et al. [37],Luimes et al. [38], material degradation due to biogenic sulphide corrosion may reduce the load bearing capacity of concrete sewer pipes by more than a factor two. Hence, it is important that municipalities regularly monitor the evolution of the effective wall thickness of (especially older) concrete sewer pipes. This may be done by core sampling of *in-situ* sewer pipes, and subjecting these samples to a similar set of experiments as proposed in the present work. In addition, the laser profiling technique recently developed by Clemens et al. [75] may help to monitor a decrease in wall thickness due to degradation by biogenic sulphide corrosion. For an adequate assessment of pipe degradation, prior to pipe installation characteristic data of sewer pipes should be recorded, such as the topology and dimensions of the sewer pipes, the concrete composition, the presence of characteristic chemical compounds, the concrete and sewer pipe design strength classes, and the environmental design class.

- The values and time-dependent trends found for the concrete properties and corrosion depths of domestic sewer pipes can serve as input for practical analyses and advanced numerical simulations on their bearing capacity and time-dependent degradation, see, e.g., Scheperboer et al. [37] and Luimes et al. [38]. It is important that the significant spread in the experimental values is hereby accounted for, as induced by variations in the material composition of sewer pipes and the local environmental conditions experienced.

The above conclusions and practical recommendations can be incorporated into the assessment of the physical condition of concrete sewer systems applied in domestic service locations. In this way, a scientific basis is created for improving decision-making processes of municipalities, water boards, and production, engineering and research companies, about maintenance, remediation and replacement of concrete sewage systems. This should support an efficient sewer system asset management, with minimal financial costs and societal impact.

CRediT authorship contribution statement

R.A. Luimes: Conceived the experiments and numerical simulations, Performed the experiments and numerical simulations, Writing – original draft. **I.C. Scheperboer:** Conceived the experiments and numerical simulations, Performed the experiments and numerical simulations, Writing – original draft. **A.S.J. Suiker:** Conceived the experiments and numerical simulations, Writing – original draft. **E. Bosco:** Conceived the experiments and numerical simulations, Writing – original draft. **F.H.L.R. Clemens:** Conceived the experiments, Writing – review & editing.

Declaration of competing interest

The authors declare that they have no known competing financial interests or personal relationships that could have appeared to influence the work reported in this paper.

Data availability

Data will be made available on request.

Acknowledgements

References

[1] Oosterom GE, Hermans RHJJ. Rioleringsatlas van Nederland: voorzieningen, beheer en financiën in beeld. Ede: Stichting Rioned; 2005.

[2] Stanić N, de Haan C, Tirion M, Langeveld JG, Clemens FHLR. Comparison of core sampling and visual inspection for assessment of concrete sewer pipe condition. Water Sci Technol 2013;67:2458–66.

[3] Dirksen J, Clemens FHLR, Korving H, Cherqui F, Le Gauffre P, Ertl T, et al. The consistency of visual sewer inspection data. Struct Infrastructure Eng 2013;9:214–28.

[4] Davies PJ, Clarke BA, Whiter JT, Cunningham RJ, Leidi A. The structural condition of rigid sewer pipes: a statistical investigation. Urban Water 2001;3(4):277–86.

[5] Wirahadikusumah R, Abraham D, Iseley T. Challenging issues in modeling deterioration of combined sewers. J Infrastructure Syst 2001;7:77–84.

[6] Stanić N, Langeveld J, Salet T, Clemens F. Relating the structural strength of concrete sewer pipes and material properties retrieved from core samples. Struct Infrastructure Eng 2017;13(5):637–51.

[7] Ana E, Bauwens W, Pessemier M, Thoeye C, Smolders S, Boonen I, et al. An investigation of the factors influencing sewer structural deterioration. Urban Water J 2009;6(4):303–12.

[8] Davies PJ, Clarke BA, Whiter JT, Cunningham RJ. Factors influencing the structural deterioration and collapse of rigid sewer pipes. Urban Water 2001;3(1–2):73–89.

[9] Grengg C, Mittermayr F, Ukrainczyk N, Koraimann G, Kienesberger S, Dietzel M. Advances in concrete materials for sewer systems affected by microbial induced concrete corrosion: A review. Water Res 2018;134:341–52.

[10] Parker CD. The corrosion of concrete: 1. The isolation of a species of bacterium associated with the corrosion of concrete exposed to atmospheres containing hydrogen sulphide. J Australas Soc Immunol 1945;23(2):81–90.

[11] Monteny J, Vincke E, Beeldens A, de Belie N, Taerwe L, van Gemert D, et al. Chemical, microbiological, and in situ test methods for biogenic sulfuric acid corrosion of concrete. Cem Concr Res 2000;30:623–34.

[12] Gu L, Visintin P, Bennett T. Evaluation of accelerated degradation test methods for cementitious composites subject to sulfuric acid attack; application to conventional and alkali-activated concretes. Cem Concr Res 2018;87:187–204.

[13] Wells T, Melchers RE. An observation-based model for corrosion of concrete sewers under aggressive conditions. Cem Concr Res 2014;61–62:1–10.

[14] Wells T, Melchers RE. Modelling concrete deterioration in sewers using theory and field observations. Cem Concr Res 2015;77:82–96.

[15] Allahverdi A, Škvára F. Acidic corrosion of hydrated cement based materials part 2. - Kinetics of the phenomenon and mathematical models. Ceramics 2000;44(4):152–60.

[16] Rooyackers FAM, Bosco E, Suiker ASJ, Clemens FHLR. A chemo-mechanical model for biogenic sulphide corrosion of concrete. Cem Concr Res 2022;160:106809.

[17] Davis JL, Nica D, Shields K, Roberts DJ. Analysis of concrete from corroded sewer pipe. Int Biodeterioration Biodegrad 1998;42:75–84.

[18] Grengg C, Mittermayr F, Baldermann A, Böttcher ME, Leis A, Koraimann G, et al. Microbiologically induced concrete corrosion: A case study from a combined sewer network. Cem Concr Res 2015;77:16–25.

[19] Islander RL, Devinny JS, Mansfeld F, Postyn A, Shih H. Microbial ecology of crown corrosion in sewers. J Environ Eng 1991;117(6):751–70.

[20] Roberts DJ, Nica D, Zuo G, Davis JL. Quantifying microbially induced deterioration of concrete: initial studies. Int Biodeterioration Biodegrad 2002;49:227–34.

[21] Jiang G, Wightman E, Donose BC, Yuan Z, Bond PL, Keller J. The role of iron in sulfide induced corrosion of sewer concrete. Water Res 2014;49:166–74.

[22] Oualit M, Jauberthie R, Rendell F, Melinge Y, Abadlia MT. External corrosion to concrete sewers: a case study. Urban Water J 2012;9(6):429–34.

[23] Marquez-Peñaranda JF, Sanchez-Silva M, Husserl J, Bastidas-Arteaga E. Effects of biodeterioration on the mechanical properties of concrete. Mater Struct 2016;49:4085–99.

[24] Bosco E, Claessens RJMA, Suiker ASJ. Multi-scale prediction of chemo-mechanical properties of concrete materials through asymptotic homogenization. Cem Concr Res 2020;128:105929.

[25] Šavija B, Luković M. Carbonation of cement paste: Understanding, challenges, and opportunities. Constr Build Mater 2016;117:285–301.

[26] Hill JJ, Kurdziel JM, Nelson CR, Nystrom JA, Sondag MS. Minnesota department of transportation overload field tests of standard and standard installation direct design reinforced concrete pipe installations. Transp Res Rec J Transp Res Board 1999;1656:64–72.

[27] McGrath TJ, Selig ET, Webb MC, Zoladz GV. Pipe interaction with the backfill envelope. McLean, VA: US Department of Transportation; 1999, p. 269.

[28] Brachman RWI, Moore ID, Rowe RK. The performance of a laboratory facility for evaluating the structural response of small-diameter buried pipes. Can Geotech J 2001;38:260–75.

[29] Zoladz GV, McGrath TJ, Selig ET. Laboratory tests of buried pipe installation procedures. Transp Res Rec J Transp Res Board 1996;1541:86–96.

[30] Zamanian S, Hur J, Shafieezadeh A. A high-fidelity computational investigation of buried concrete sewer pipes exposed to truckloads and corrosion deterioration. Eng Struct 2020;221:111043.

[31] Peter JM, Chapman D, Moore ID, Hoult N. Impact of soil erosion voids on reinforced concrete pipe responses to surface loads. Tunn Undergr Space Technol 2018;82:111–24.

[32] Meguid MA, Kamel S. A three-dimensional analysis of the effects of erosion voids on rigid pipes. Tunn Undergr Space Technol 2014;43:276–89.

[33] Tan Z. Nonlinear finite element study of deteriorated sewers including the influence of erosion voids [Ph.D. thesis], Kingston, Ontario, Canada: Queen's University; 2007.

[34] Xu M, Shen D. The influence of erosion voids on the longitudinal behaviour of a jointed large-diameter reinforced concrete pipeline. Tunn Undergr Space Technol 2020;103:103494.

[35] Scheperboer IC, Suiker ASJ, Bosco E, Clemens FHLR. A coupled hydro-mechanical model for subsurface erosion with analyses of soil piping and void formation. Acta Geotech 2022;17:4769–98.

[36] Rakitin B, Xu M. Centrifuge modeling of large-diameter underground pipes subjected to heavy traffic loads. Can Geotech J 2014;51:353–68.

[37] Scheperboer IC, Luimes RA, Suiker ASJ, Bosco E, Clemens FHLR. Experimental-numerical study on the structural failure of concrete sewer pipes. Tunn Undergr Space Technol 2021;116:104075.

[38] Luimes RA, Scheperboer IC, Suiker ASJ, Bosco E, Clemens FHLR. Effect of biochemical attack on the mechanical performance of used concrete sewer pipes. Constr Build Mater 2022;346:128390.

[39] European Committee for Standardization. NEN-EN 206 + NEN 8005 - Concrete - Specification, performance, production and conformity + Dutch supplement to NEN-EN 206. 2017.

[40] Gutberlet T, Hilbig H, Beddoe RE. Acid attack on hydrated cement - Effect of mineral acids on the degradation process. Cem Concr Res 2015;74:35–43.

[41] Monteny J, De Belie N, Taerwe L. Resistance of different types of concrete mixtures to sulfuric acid. Mater Struct 2003;36:242–9.

[42] Vereniging van Producenten van Betonleidingsystemen VPB. Handboek betonnen buizen. Amsterdam: Vereniging van Producenten van Betonleidingsystemen VPB; 1979.

[43] Vollertsen J, Nielsen AH, Jensen HS, Wium-Andersen T, Hvitved-Jacobsen T. Corrosion of concrete sewers - the kinetic of hydrogen sulfide oxidation. Sci Total Environ 2008;394:162–70.

[44] European Committee for Standardization. NEN-EN 13508-2 - Investigation and assessment of drain and sewer systems outside buildings - part 2: Visual inspection coding system. 2021.

[45] RILEM TC 56-MHM. CPC-18 Measurement of hardened concrete carbonation depth. Mater Struct 1988;21(126):453–5.

[46] Thiery M, Villain G, Dangla P, Platret G. Investigation of the carbonation front shape on cementitious materials: Effects of the chemical kinetics. Cem Concr Res 2007;37:1047–58.

[47] Papadakis VG, Fardis MN, Vayenas CG. Effect of composition, environmental factors and cement-lime mortar coating on concrete carbonation. Mater Struct 1992;25:293–304.

[48] O'Connell M, McNally C, Richardson MG. Biochemical attack on concrete in wastewater applications: A state of the art review. Cem Concr Compos 2010;32:479–85.

[49] Rimmelé G, Barlet-Gouédard V, Porcherie O, Goffé B, Brunet F. Heterogeneous porosity distribution in Portland cement exposed to CO_2-rich fluids. Cem Concr Res 2008;38:1038–48.

[50] Castellote M, Andrade C. Modelling the carbonation of cementitious matrixes by means of the unreacted-core model, UR-CORE. Cem Concr Res 2008;38:1374–84.

[51] European Committee for Standardization. NEN-EN 12390-13 - Testing hardened concrete - part 13: Determination of secant modulus of elasticity in compression. 2013.

[52] European Committee for Standardization. NEN-EN 12390-3 - Testing hardened concrete - part 3: Compressive strength of test specimens. 2019.

[53] Luimes RA, Suiker ASJ, Verhoosel CV, Jorissen AJM, Schellen HL. Fracture behaviour of historic and new oak wood. Wood Sci Technol 2018;52:1243–69.

[54] Xu XP, Needleman A. Numerical simulations of fast crack growth in brittle solids. J Mech Phys Solids 1994;42:1397–407.

[55] Cid Alfaro MV, Suiker ASJ, de Borst R. Transverse failure behavior of fiber-epoxy systems. J Compos Mater 2010;44:1493–516.

[56] Cid Alfaro MV, Suiker ASJ, Verhoosel CV, de Borst R. Numerical homogenization of cracking processes in thin fibre-epoxy layers. Eur J Mech A Solids 2010;29:119–31.

[57] Cid Alfaro MV, Suiker ASJ, de Borst R, Remmers JJC. Analysis of fracture and delamination in laminates using 3D numerical modelling. Eng Fract Mech 2009;76:761–80.

[58] Scheperboer IC, Suiker ASJ, Luimes RA, Bosco E, Jorissen AJM. Collapse response of two-dimensional cellular solids by plasticity and cracking: application to wood. Int J Fract 2019;219:221–44.

[59] Luimes RA, Suiker ASJ. Numerical modelling of climate-induced fracture and deformation in wood: Application to historical museum objects. Int J Solids Struct 2021;210–211:237–54.

[60] Eumelen GJAM, Bosco E, Suiker ASJ, van Loon A, Iedema PD. A computational model for chemo-mechanical degradation of historical paintings due to metal soap formation. J Mech Phys Solids 2019;132:103683.

[61] Eumelen GJAM, Bosco E, Suiker ASJ, Hermans JJ, van Loon A, Keune K, et al. Computational modelling of metal soap formation in historical oil paintings: the influence of fatty acid concentration and nucleus geometry on the induced chemo-mechanical damage. SN Appl Sci 2020;2:1310.

[62] Eumelen GJAM, Bosco E, Suiker ASJ, Hermans JJ. Chemo-mechanical model for degradation of oil paintings by amorphous and crystalline metal soaps. Eur J Mech A Solids 2023;97:104827.

[63] Forschelen PJJ, Suiker ASJ, van der Sluis O. Effect of residual stress on the delamination response of film-substrate systems under bending. Int J Solids Struct 2016;97–98:284–99.

[64] Geng F, Suiker ASJ. An interface model for high-cycle fatigue. Eng Fract Mech 2019;221:106644.

[65] European Committee for Standardization. NEN-EN 1992-1-1 - Eurocode 2: Design of concrete structures - Part 1-1: General rules and rules for buildings. 2005.

[66] Reinhardt HW, Xu S. A practical testing approach to determine mode II fracture energy G_{11F} for concrete. Int J Fract 2000;105:107–25.

[67] Mori T, Nonaka T, Tazaki K, Koga M, Hikosaka Y, Noda S. Interactions of nutrients, moisture and pH on microbial corrosion of concrete sewer pipes. Water Res 1992;26:29–37.

[68] Ayoub GM, Azar N, El Fadel M, Hamad B. Assessment of hydrogen sulphide corrosion of cementitious sewer pipes: a case study. Urban Water J 2004;1:39–53.

[69] Vincke E, Boon N, Verstraete W. Analysis of the microbial communities on corroded concrete sewer pipes - a case study. Appl Microbiol Biotechnol 2001;57:776–85.

[70] Cwalina B. Biodeterioration of concrete. Archit Civ Eng Environ 2008;4:133–40.

[71] Hu S, Chen Q, Gong N. Effect of acid corrosion on crack propagation of concrete beams. Sãdhanã 2018;43(23):1–13.

[72] Fan YF, Hu ZQ, Zhang YZ, Liu JL. Deterioration of compressive property of concrete under simulated acid rain environment. Constr Build Mater 2010;24:1975–83.

[73] Ortega J, García-Vera V, Solak A, Tenza-Abril A. Pore structure degradation of different cement mortars exposed to sulphuric acid. Appl Sci 2019;9:1–13.

[74] Khalilpour S, BaniAsad E, Dehestani M. A review on concrete fracture energy and effective parameters. Cem Concr Res 2019;120:294–321.

[75] Clemens F, Stanić N, Van der Schoot W, Langeveld J, Lepot M. Uncertainties associated with laser profiling of concrete sewer pipes for the quantification of the interior geometry. Struct Infrastructure Eng 2015;11(9):1218–39.